CrossMark

Dark current transport mechanism associated with acceptor concentration in GaAs-based blocked-impurity-band (BIB) detectors

Xiaodong Wang[1] (ID) · Yulu Chen[1] · Xiaoyao Chen[2] · Bingbing Wang[1] ·
Chuansheng Zhang[1] · Haoxing Zhang[1] · Ming Pan[1]

Abstract Dark current transport mechanism associated with acceptor concentration in GaAs-based blocked-impurity-band (BIB) detectors has been investigated. Device structure, numerical models and simulation techniques are described in detail. By careful model and parameter calibration, the numerical simulation is completely consistent with the analytical calculation, proving the validity of simulation methods. Our results reveals that the carrier-transport modes of GaAs-based BIB detectors can be classified into two categories (i.e., electron current and hopping current), and the hopping current can be neglected compared with the electron current. Besides, it is demonstrated that the dark current of GaAs-based BIB detector is dominated by the drift–diffusion current and the generation-recombination current, and the both current components are monotonically decreasing functions of the acceptor concentration.

✉ Yulu Chen
  yukiylc@163.com

✉ Xiaoyao Chen
  chenxiaoyao@fudan.edu.cn

[1] The 50th Research Institute of China Electronics Technology Group Corporation, 318 Chang He Road, Shanghai 200331, China

[2] Laboratory of Advanced Material, Fudan University, Shanghai 200438, China

1 Introduction

Terahertz (THz) radiation is commonly known as the electromagnetic wave with frequency range from 0.3 to 10 THz. Within the electromagnetic spectrum, it lies in the spectral band between the microwave and the infrared. The importance of THz technology (Tonouchi 2007; Siegel 2002) has been recognized by more and more people due to the following advantages: strong penetration, good safety, high resolution, and excellent directionality. Nowadays, the THz technology can be widely used in the imaging and spectrum application area (Mittleman et al. 1996; Liu et al. 2007), especially in the security check, nondestructive testing, material identification, atmospheric monitoring, and astronomical observation. For instance, CETC50 (Zhou et al. 2017) has developed a dual-band terahertz imaging system as a potential product for nondestructive testing using heterodyne detectors and continuous-wave sources; University of Shanghai for science and technology (Shi et al. 2016) has proposed a compact broadband terahertz perfect absorber as a potential application in imaging and anti-radar cloaking devices. The key factor which determines the application of THz technology is high-performance THz detectors, and thus the development of high-performance THz detectors has become the leading force driving the THz technology forward. Blocked impurity band (BIB) detector is a member in the family of opto-electronic THz detectors, and it is more popular than $Hg_{1-x}Cd_xTe$ photovoltaic detectors (Hu et al. 2014) due to the weak Hg–Te bond, uniformity and yield still encountered by $Hg_{1-x}Cd_xTe$ epitaxial material. BIB detectors can be classified into Si-based and GaAs-based BIB detectors. Si-based BIB detectors have the advantages including high response sensitivity, large array scale, and wide detection spectrum, and have realized a certain degree of application in the field of space-based, and high altitude land-based, and air-borne THz detection systems. For examples, The ISO satellite launched by the ESA has adopted the 1×12 Si-based BIB detectors in 1995, SIRTF satellite launched by the NASA has adopted the 128×128 Si-based BIB detectors in 2003, and ASTRO-F satellite launched by Japan has adopted the 256×256 Si-based BIB detectors in 2004.

GaAs-based BIB detectors (Reichertz et al. 2006) can response the THz wavelength beyond 500 μm (corresponding to 0.6 THz), and thus it has attracted worldwide attentions since the first prototype of GaAs-based BIB detector (Reichertz et al. 2005) has been successfully developed. However, due to the restriction from the material crystalline quality and device processing technique, the research on GaAs-based BIB detector is still on the initial stage. Until now, GaAs-based BIB focal plane arrays have not been reported, and the problems of poor reproducibility, large dark current, and low responsivity are still encountered by the single-element detector, blocking the application of GaAs-based BIB detectors.

Acceptor impurity is unintentionally introduced into the N-type GaAs material during the process of epitaxy. Acceptor concentration as an important parameter to evaluate the quality of GaAs epitaxial material can dramatically influence the carrier transport characteristics of GaAs-based BIB detectors. In order to determine the bottlenecks of restricting the device performance from achieving a higher level, it is worthwhile investigating the dark current transport mechanism associated with the acceptor concentration in GaAs-based BIB detectors. The motivation of this work is as follows: On one hand, dark current is a key parameter to characterize the device performance, which can directly determine the dynamic range of the detector; On the other hand, Reichertz et al. in the UC Berkeley (2005) has reported that the depletion width is a monotonically decreasing function of the accept concentration (N_A), and thus it seems that a lower N_A is preferred. However, the

effect of acceptor concentration on the dark current characteristics has not been reported yet. Therefore, a comprehensive design consideration for the optimal N_A is still missing.

2 Device structure and simulation models

Figure 1 shows the structural model of GaAs-based BIB THz detector. From the bottom to the top, the detailed device structure is as follows: (1) the conducting GaAs substrate with donor concentration of 5×10^{18} cm^{-3}; (2) the absorbing layer and the blocking layer sequentially formed by epitaxial technique with donor concentration of 5×10^{15} and 1×10^{13} cm^{-3}, respectively; (3) the contact layer formed by ion implantation with donor concentration of 3×10^{19} cm^{-3}; (4) the anode formed upon the contact layer; (5) the cathode formed upon the substrate. The anode and cathode constitute jointly the detector electrodes. In order to show the relationship between the different photosensitive elements, structural model shown in Fig. 1 has two discrete mesa-type pixels with the only one cathode. Besides, it is reasonable to assume in our simulation that all the epitaxial layers including the absorbing layer and the blocking layer have the same acceptor concentration because the acceptor impurities are unintentionally introduced into GaAs regardless of the specific epitaxial layer.

The physical models involved in the simulation of GaAs-based BIB detectors have been described elsewhere (Wang et al. 2011, 2012, 2014, 2016a), and the impurity band can be established between the conduction band and the valance band by the physical model construction. The photoresponse process of GaAs-based BIB detector is as follows: (1) THz wave is front-illuminated on the detector; (2) THz wave pass through the contact layer and the blocking layer, and then is absorbed by the absorbing layer; (3) Photo-generated carriers travel along the bent conduction band, and eventually are collected by the electrodes.

3 Results and discussion

In the following section, our discussion will focus primarily on the dark current transport mechanism associated with the acceptor concentration in GaAs-based BIB detectors. Figure 6 presents the dark current as a function of anode bias with acceptor concentration (N_A) increasing from 2×10^{11} to 1×10^{13} cm^{-3}. It is found that dark current keeps a

Fig. 1 Schematic cross-section of GaAs-based BIB THz detector
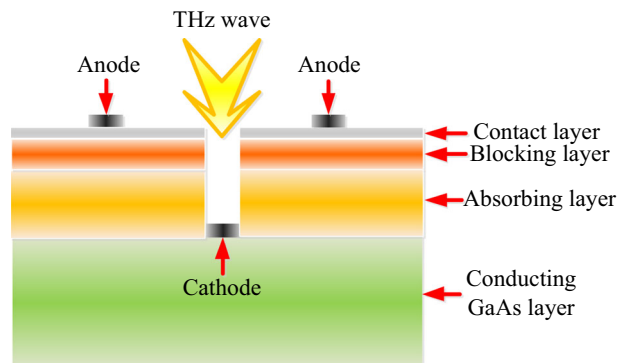
relatively small value when the anode bias (V_A) is below a certain value, which can be represented by the threshold voltage (V_T). When $V_A > V_T$, the dark current is exponentially increasing with V_A first, and then is linearly increasing with V_A, and finally is saturated to a certain value which is independent of V_A. Besides, as for a fixed bias voltage, a larger N_A can lead to a lower dark current level. The inset of Fig. 2 shows the relationship between V_T and N_A. It is interesting to note that V_T is nearly a linearly increasing function of N_A, which indicating a certain V_T can be customized for GaAs-based BIB detector by controlling N_A during the epitaxy. In order to elucidate dark current transport mechanism associated with N_A, it is necessary to explore the dependence of carrier transport process on N_A.

In our previous work (Wang et al. 2016b), it has been demonstrated that the carrier-transport modes of GaAs-based BIB detectors can be classified into two categories (i.e., electron current and hopping current). The electron current is originated from drift process of thermally excited electrons in conduction band, and the hopping current is originated from the hopping process of bound electrons through vacancies in the impurity band. The current–voltage characteristics of BIB detector is much like a photodiode, in which the drift–diffusion current and the generation-recombination (g–r) current (Qiu et al. 2015, 2016) can dominate the dark current mechanism at low-bias region. It is known that the drift–diffusion current (I_{diff}) has the following form:

$$I_{diff} = Aqn_i^2 \sqrt{\frac{KT}{q}} \left(\sqrt{\frac{\mu_n}{\tau_n}} \cdot \frac{1}{N_A} + \sqrt{\frac{\mu_v}{\tau_v}} \cdot \frac{1}{N_D} \right) \cdot \left[\exp\left(\frac{qV_d}{kT} \right) - 1 \right] \tag{1}$$

where A is the photosensitive area; q is the unit electronic charge; n_i is the intrinsic carrier concentration; K is the Boltzmann constant; T is the device temperature; N_A and N_D are acceptor and donor concentration, respectively; V_a is the applied bias voltage; t_n is the electron lifetime and μ_n is the electron mobility, and; t_v is the vacancy lifetime and μ_v is the vacancy mobility. Because N_A is commonly three orders of magnitude lower than N_D (Wang et al. 2015), Eq. (1) can be simplified as:
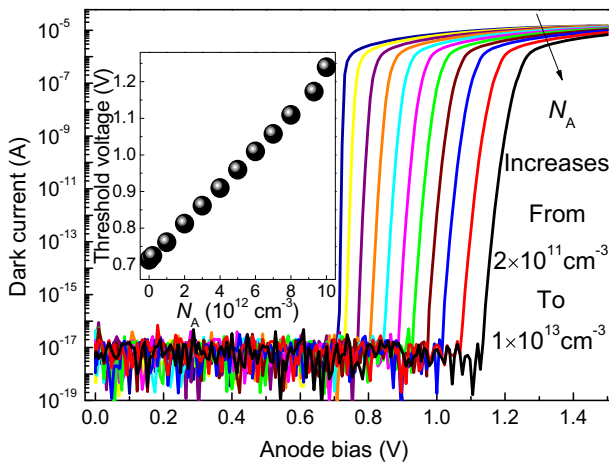

Fig. 2 Dark current as a function of anode bias for different N_A. Inset shows the relationship between V_T and N_A

$$I_{diff} = Aqn_i^2\sqrt{\frac{KT}{q}} \cdot \sqrt{\frac{\mu_n}{\tau_n}} \cdot \frac{1}{N_A} \cdot \left[\exp\left(\frac{qV_a}{kT}\right) - 1\right] \tag{2}$$

All the physical quantities except μ_n in Eq. (2) are independent of N_A, and thus Eq. (2) reduces to:

$$I_{diff} \propto \frac{\sqrt{\mu_n}}{N_A} \tag{3}$$

Figure 2 shows the vertical distributions of electron mobility with N_A increasing from 2×10^{11} to 1×10^{13} cm^{-3}. It is noted that μ_n in the blocking layer is a monotonically decreasing function of N_A, while μ_n in the absorbing layer is a monotonically increasing function of N_A instead. In this paper, our discussion is only concentrated on the physical processes occurring in the absorbing layer due to the absence of carrier generation in the blocking layer. It can be found from Fig. 3 that although μ_n can increase with the increased N_A, the increasing extent of N_A is far beyond that of $\mu_n^{1/2}$. Therefore, I_{diff} is a monotonically decreasing function of N_A according to Eq. (3).

The g–r current is caused by the g–r centers in the depletion region, and can be expressed as:

$$I_{g-r} = \frac{qn_iAW}{\tau_{eff}}\left[\exp\left(\frac{qV}{2KT}\right) - 1\right] \tag{4}$$

where W is the width of depletion region, and; τ_{eff} is the effective carrier lifetime, which is determined jointly by Shockley–Read–Hall, Radiative, and Auger recombination. Actually, the formulations of depletion-region width and electric-field intensity of an n-type BIB detector have been deduced using analytical method (Cardozo 2004), and are given by:
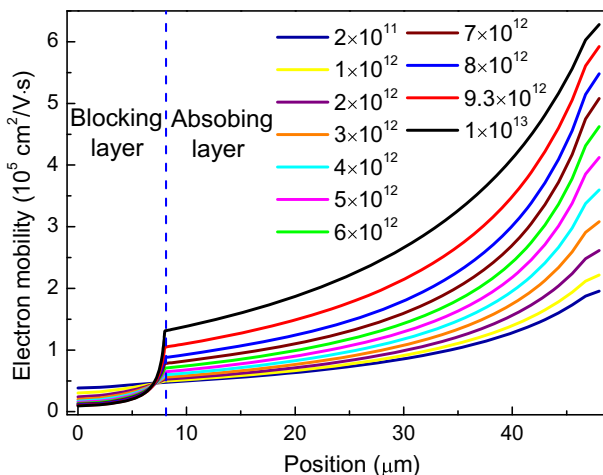

Fig. 3 Vertical profiles of electron mobility at 1.5 V for different N_A

$$W = \sqrt{\frac{2\varepsilon\varepsilon_0(V_a - V_{bi})}{qN_A} + b^2} - b \tag{5}$$

$$E(x) = \frac{qN_A}{\varepsilon\varepsilon_0}[W - x] \tag{6}$$

where ε is the relative dielectric constant; ε_0 is the permittivity of free space; V_{bi} is the built-in potential, and; b is the thickness of blocking layer. The simulated vertical profiles of electric field for different N_A are shown in Fig. 4. The origin of abscissa represents the interface between the anode and the blocking layer, where the electric-field intensity can be obtained by substituting Eq. (5) into Eq. (6):

$$E(0) = \frac{1}{\varepsilon\varepsilon_0} \cdot \left[\sqrt{2q\varepsilon\varepsilon_0(V_a - V_{bi})N_A + (qbN_A)^2} - qbN_A \right] \tag{7}$$

Comparing the numerically simulated electric-field profiles in Fig. 4 with the analytical results [i.e., Eqs. (5)–(7)], it is demonstrated that the numerical simulation is completely consistent with the analytical calculation, proving the validity of simulation methods. Specifically, (1) the depletion-region width is a decreasing function of N_A, which is consistent with Eq. (5); (2) electric field in the interface between the anode and the blocking layer is a monotonically increasing function of N_A, which is consistent with Eq. (7). Taking Fig. 4 and Eq. (4) into consideration, it is clear that an increase of N_A can result in a decrease in I_{g-r}.

Based on the above discussion, it can be concluded that the dark current of GaAs-based BIB detector is dominated by drift–diffusion current and generation-recombination current, and the both current components are monotonically decreasing functions of N_A. This conclusion can well explain the simulation results shown in Fig. 2. The above discussion, particularly in relation to drift–diffusion current, has assumed that the hopping current originating from the hopping process of bound electrons through vacancies in the impurity band is so small that it can be neglected. In order to prove this assumption by numerical
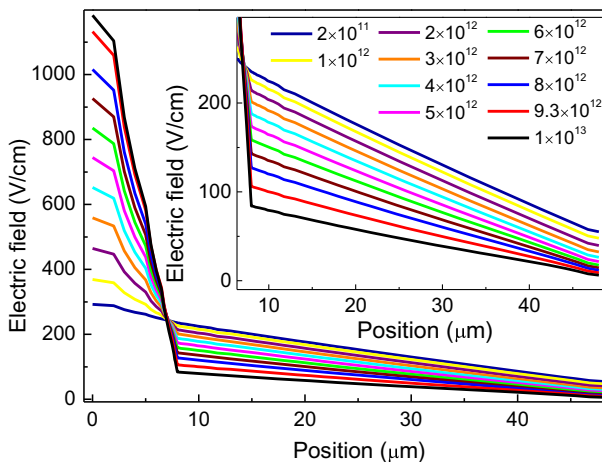

Fig. 4 Vertical profiles of electric field at 1.5 V for different N_A. Inset shows the enlarged electric-field distributions in the absorbing layer
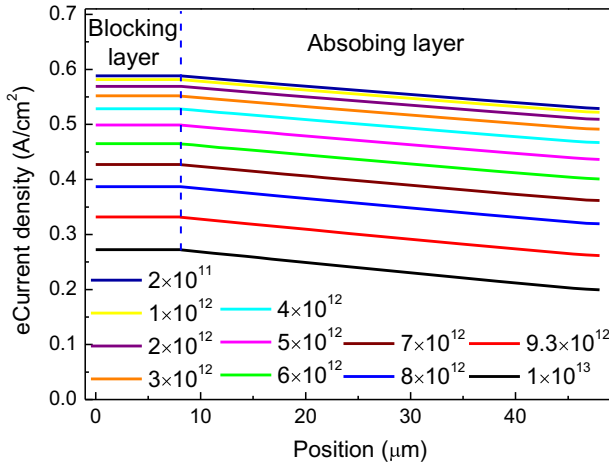
Fig. 5 Vertical distributions of electron current density at 1.5 V for different N_A
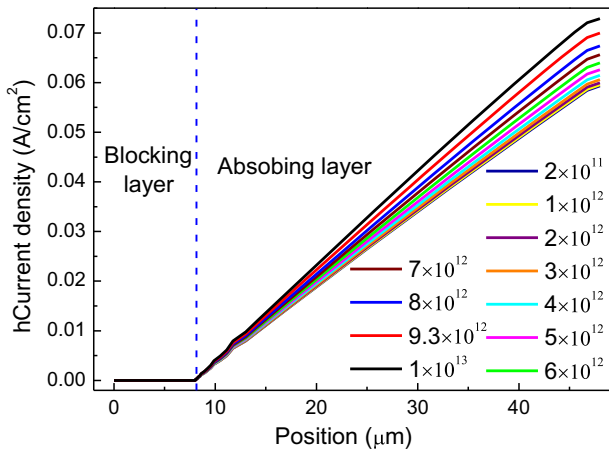

Fig. 6 Vertical distributions of hopping current density at 1.5 V for different N_A

simulation, the effects of N_A on the vertical distributions of electron current density, hopping current density and total current are investigated, respectively. As shown in Figs. 5 and 6, the hopping current density is almost one order of magnitude lower than electron current density.

Besides, a larger N_A can lead to a lower electron current density according to Fig. 5, while giving rise to a higher hopping current density according to Fig. 6. Adding electron current density in Fig. 5 and hopping current density in Fig. 6 together, total current density can be obtained. As presented in Fig. 7, the total current density is uniform along the vertical direction, which confirms the fact that the carrier-transport modes of GaAs-based BIB detectors can be classified into electron current and hopping current. Comparison between Figs. 5 and 7 reveals that the electron current density and the total current
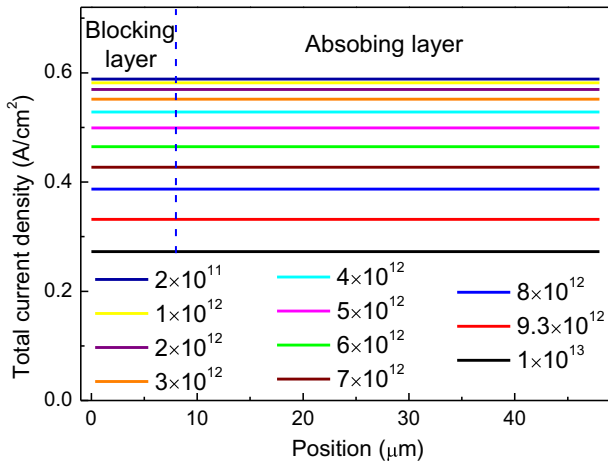
Fig. 7 Vertical distributions of total current density at 1.5 V for different N_A

density are nearly the same in magnitude, and they are both monotonically decreasing functions of N_A, which confirms the fact that hopping current can be neglected compared with the electron current.

4 Conclusion

In this paper, dark current transport mechanism associated with acceptor concentration in GaAs-based blocked-impurity-band (BIB) detectors has been investigated. The numerical simulation is completely consistent with the analytical calculation, proving the validity of simulation methods. Our results reveal that the carrier-transport modes of GaAs-based BIB detectors can be classified into two categories (i.e., electron current and hopping current), and the hopping current can be neglected compared with the electron current. It is demonstrated that the dark current of GaAs-based BIB detector is dominated by the drift–diffusion current and the generation-recombination current, and the both current components are monotonically decreasing functions of the acceptor concentration.

References

Cardozo, B.L.: GaAs blocked-impurity-band detectors for far-infrared astronomy. Doctoral thesis, University of California, Berkeley (2004)

Hu, W., Ye, Z., Liao, L., Chen, H., Chen, L., Ding, R., He, L., Chen, X., Lu, W.: A 128 × 128 long wave length/mid-wavelength two-color HgCdTe infrared focal plane array detector with ultra-low spectral crosstalk. Opt. Lett. **39**, 5130–5133 (2014)

Liu, H.B., Zhong, H., Karpowicz, N., Chen, Y.Q., Zhang, X.C.: Terahertz spectroscopy and imaging for defense and security applications. Proc. IEEE **95**, 1514–1527 (2007)

Mittleman, D.M., Jacobsen, R.H., Nuss, M.C.: T-ray imaging. IEEE J. Sel. Top. Quantum Electon. **2**, 679–692 (1996)

Qiu, W.C., Hu, W.D., Chen, L., Lin, C., Cheng, X.A., Chen, X.S., Lu, W.: Dark current transport and avalanche mechanism in HgCdTe electron-avalanche photodiodes. IEEE Trans. Electron Devices **62**, 1926–1931 (2015)

Qiu, W.C., Hu, W.D., Lin, C., Chen, X.S., Lu, W.: Surface leakage current in 12.5 μm long-wavelength HgCdTe infrared photodiode arrays. Opt. Lett. **41**, 828–831 (2016)

Reichertz, L.A., Cardozo, B.L., Beeman, J.W., Larsen, D.I., Tschanz, S., Jakob, G., Katterloher, R., Haegel, N.M., Haller, E.E.: First results on GaAs blocked impurity band (BIB) structures for far-infrared detector arrays. In: Proceedings of SPIE, vol. 5883, p. 58830Q (2005)

Reichertz, L.A. Beeman, J.W., Cardozo, B.L., Jakob, G., Katterloher, R., Haegel, N.M., Haller, E.E.: Development of a GaAs based BIB detector for sub-mm wavelengths. In: Proceedings of SPIE, vol. 6275, p. 62751S (2006)

Shi, C., Zang, X.F., Chen, L., Peng, Y., Cai, B., Nash, G.R., Zhu, Y.M.: Compact broadband terahetz perfect absorber based on multi-interference and diffraction effects. IEEE Trans. THz Sci. Technol. **6**, 40–44 (2016)

Siegel, P.H.: Terahertz technology. Nature **50**, 910–928 (2002)

Tonouchi, M.: Cutting-edge terahertz technology. Nat. Photon. **1**, 97–105 (2007)

Wang, X., Hu, W., Chen, X., Xu, J., Wang, L., Li, X., Lu, W.: Dependence of dark current and photoresponse characteristics on polarization charge density for GaN-based avalanche photodiodes. J. Phys. D Appl. Phys. **44**, 405102-1–405102-11 (2011)

Wang, X.D., Hu, W.D., Chen, X.S., Lu, W.: The study of self-heating and hot-electron effects for AlGaN/GaN double-channel HEMTs. IEEE Trans. Electron Devices **59**, 1393–1401 (2012)

Wang, X.D., Hu, W.D., Pan, M., Hou, L.W., Xie, W., Xu, J.T., Li, X.Y., Chen, X.S., Lu, W.: Study of gain and photoresponse characteristics for back-illuminated separate absorption and multiplication GaN avalanche photodiodes. J. Appl. Phys. **115**, 013103-1–013101-8 (2014)

Wang, X., Wang, B., Hou, L., Xie, W., Chen, X., Pan, M.: Design consideration of GaAs-based blocked-impurity-band detector with the absorbing layer formed by ion implantation. Opt. Quantum Electron. **47**, 1347–1355 (2015)

Wang, X., Wang, B., Chen, Y., Hou, L., Xie, W., Chen, X., Pan, M.: Spectral response characteristics of novel ion-implanted planar GaAs blocked-impurity-band detectors in the terahertz domain. Opt. Quantum Electron. **48**, 518 (2016a)

Wang, X., Wang, B., Chen, X., Chen, Y., Hou, L., Xie, W., Pan, M.: Roles of blocking layer and anode bias in processes of impurity-band transition and transport for GaAs-based blocked-impurity-band detectors. Infrared Phys. Technol. **79**, 165–170 (2016b)

Zhou, D., Hou, L., Xie, W., Zang, Y., Lu, B., Chen, J., Wu, P.: Practical dual-band terahertz imaging system. Appl. Opt. **56**, 3148–3154 (2017)